Microwave assisted solution synthesis, structural, morphological, optical, electrical properties of tin oxide (SnO_2) nanoparticles

R. ANITHA[a], E. KUMAR[b,*], S. C. VELLA DURAI[c], M. VARGHEESE[d]
[a]*Bharathiar University,Coimbatore, Tamilnadu, India; Sri S. Ramasamy Naidu Memorial College, Sattur, Virudhunagar, Tamilnadu, India*
[b]*Department of Physics, Tamil Nadu Open University, Chennai, Tamil Nadu, India*
[c]*Department of Physics, JP College of Arts and science, Agarakattu, Tenkasi, Tirunelveli, Tamilnadu, India*
[d]*PSN College of Engineering and Technology, Melathediyur, Tirunelveli, Tamilnadu, India*

Tin Oxide (SnO_2) n-type controllable morphological structures and crystalline nanoparticles were synthesized under microwave-assisted solution method. The obtained SnO_2 nanoparticles were analyzed by powder X-ray diffraction, Fourier transforms IR spectroscopy (FTIR), UV–vis spectra (UV), High-resolution transmission electron microscopy (HRTEM), and Impedance spectroscopy. The powder XRD results clearly showed that the crystalline phase of the as-synthesized SnO_2 nanoparticles conformed to a tetragonal rutile structure and from the sharp line broadening of the XRD peak, the crystalline size was 10 - 21 nm. FTIR spectra of SnO_2 show the occurrence of anti-symmetric vibration of O–Sn–O at 620 cm^{-1}. Additionally, maximum absorption bands were observed in the room temperature UV-vis spectrum. From the HRTEM, the surface morphology of the prepared SnO_2 shows a uniformly dispersed particle, which is spherical in form. The SAED (selected area electron diffraction) pattern confirmed the pure crystalline nature of SnO_2. The AC conductivity studies showed an increase in AC conductivity value with the increase in frequency. The dielectric analysis of the prepared samples has been discussed using a dielectric constant.

(Received September 30, 2020; accepted November 24, 2021)

Keywords: Absorption, Conductivity, Crystalline, Dielectric

1. Introduction

Tin Oxide **(**SnO_2) is a notable N-type semiconducting material having a large bandgap (3.6eV) [1] and is known for different applications. A SnO_2 nanoparticle has spectacular emission property that varies from its bulk materials. The remarkable properties in different applications like gas detecting and the planning of SnO_2 nanoparticles have pulled in more consideration in the ongoing years. SnO_2 has been used as a solid sensor because of its sensitivity towards different gaseous species [2], photovoltaic energy conversion [3], etc. These days, the utilization of nanomaterials for sun-based vitality change [4] has been one of the most dynamic exploration zones in photograph catalysis [5]. Due to its specific electrical properties, tin oxide has been utilized for different electrochemical applications, such as gas sensors for ecological checking and impetuses. For such applications, the small molecule size or enormous surface territory of SnO_2 is basic for the elite. Tin Oxide semiconductor has a tetragonal rutile structure, and its lattice parameters are a = 4.738Å and c = 3.187Å [6]. So many techniques were reported for obtaining SnO_2 nanoparticles, including chemical vapour condensation [7], colloidal growth, microwave technique [8], sol-gel method [9], surfactant-assisted synthesis [10], precipitation technique [11], spray pyrolysis [12], hydrothermal synthesis [13] and laser ablation in liquids and gases [14]. Microwave-assisted synthesis is preferred among the various techniques due to its controlled grain size, morphology, and crystal structure by changing the experimental procedure. The microwave-assisted solution method has a shorter processing time and provides uniform nucleation of the powder. Since microwave-assisted synthesis is not only a rapid technique, it is cleaner, faster, and economical compared to other conventional methods. Hence this method is chosen for producing high purity SnO_2 nanoparticles for the present work. This method provides precise temperature control, high reaction rate, quality product [15], and it is environmentally friendly [16].

2. Experimental section

2.1. Preparation of tin oxide nanoparticles – microwave assisted solution method

All the chemicals involved in the microwave-assisted method were utilized as received from the substance providers without filtration and preparation. For the preparation of SnO_2 nanoparticles, 3 grams of Stannous chloride dihydrate ($SnCl_2 \cdot 2H_2O$ - AR grade) was taken, and then 5 ml ammonia was slowly mixed drop by drop

until the pH raises up to 10. At that point, the blend was kept in a stirrer for 10 minutes, at 80ºC. This arrangement was kept in a microwave and warmed for six minutes at 800 Watts (300 Hz) till the volume becomes one-fourth of its initial volume. Soon after, it was cooled for 3minutes, and the procedure was repeated once again for three minutes and stirred continuously. The acquired colloidal arrangement was separated with Whattsman channel paper. So as to eliminate the polluting influences, the arrangement was washed 2 - 3 multiple times with deionized water. To eliminate the dampness content, the wet nanoparticle was dried in the air for three days. Finally, the dried nanoparticles were grounded utilizing mortar.

2.2. Characterization techniques

The XRD technique investigated the crystal structure of the SnO_2 nanoparticles, and the data was recorded using an X-Ray Diffractometer (Bruker D8 Model) with Nickel filtered Cu - Kα radiation (λ = 1.5405Aº). Data were collected in the range of 2θ from 10º to 80º using step scan mode with a step size of 0.0170º and step time of 1s. FT-IR spectrums of the samples were recorded in the range of 400 - 4000cm^{-1}, using a Shimadzu 8400S FT-IR Spectrometer. Ultraviolet-Visible spectra of SnO_2 nanoparticles were recorded using the spectrophotometer (UV – 1800 series) in the absorption mode. The ultraviolet (UV) region was scanned from 200 to 400nm, and the visible region was scanned from 400 to 800nm. SEM image of SnO_2 nanoparticle was recorded using the Model Hitachi SEM S 2400 device at SAIF-STIC, CUSAT, Cochin. Microstructural analysis was done using HRTEM (MODEL - JOEL - J2000), operating at 200 kV at SAIF-NEHU, Shillong. The prepared samples were characterized using impedance spectroscopy. An impedance bridge (Zahner IM6) was used to measure the impedance and dielectric constants at several frequencies in the range of 10μHz to 8MHz.

3. Results and discussion

3.1. X-Ray Diffraction studies

SnO_2 nanoparticles were analyzed by powder XRD to find the structure and phase purity using an X-Ray diffractometer. The XRD of SnO_2 synthesized is shown in Fig. 1. Powder XRD results show that the sharp diffraction framed at 26.6^0, 34^0, and 51.9^0 affirmed the arrangement of SnO_2 and is crystalline in nature. All the peaks were in good concurrence with the JCPDS Card No 41-1445 as reported earlier [17, 18]. The crystallite size of SnO_2 nanoparticles was determined utilizing the estimation of FWHM from the serious XRD tops utilizing the Scherrer equation (1) [19].

$$D = \frac{K\lambda}{\beta \cos\theta} \text{ nm} \quad (1)$$

where K is a constant (0.94), λ is the wavelength (λ= 1.54059A^0), D is the crystalline size, β is the FWHM from the series of XRD tops, and θ is the angle of diffraction.

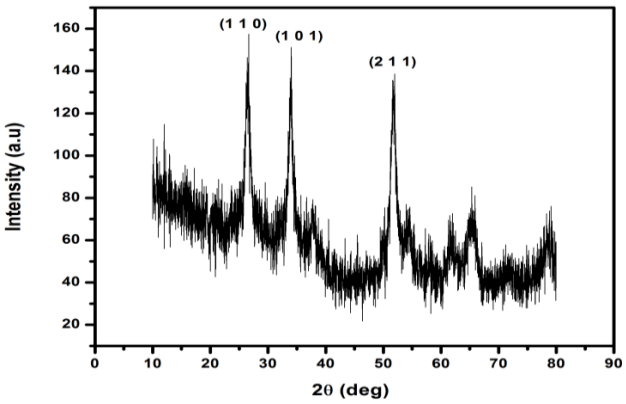

Fig. 1. XRD pattern of SnO_2 nanoparticles

SnO_2 nanocrystals synthesized by Paulo G. Mendes et al. [20] observed broader peaks [101], [110], and [211] from the XRD pattern, which indicates the nanosized nature of the tin oxide. Suraj K. Tripathy et al. [21] prepared SnO_2 material, and the material was found to be crystalline with distinct peaks at [101], [110], and [211] planes. SnO_2 nanocrystals synthesized by Krishnakumar et al. [22] found that the following miller indices, namely [101], [110], and [211] , confirm the presence of SnO_2 crystal and also matches well with JCPDS file number 41–1445. Crystalline size for SnO_2 prepared in this technique was found to be 10 - 21nm. The peak formed at 26.6^0, 34^0, and 51.9^0 can be indexed to (1 1 0), (1 0 1), (2 1 1) planes of SnO_2 crystal. The lattice parameters for the tetragonal phase structure were calculated using the relation (2) [23].

$$\frac{1}{d^2} = \frac{h^2 + k^2}{a^2} + \frac{l^2}{c^2} \quad (2)$$

The lattice parameter of the SnO_2 nano-crystal was calculated as a = 4.7 Å and c = 3.9 Å which matches well with the standard values [24].

The unit cell volume of the tetragonal lattice is given by the equation (3)

$$v = a^2.\ C = 89.86 \times 10^{-30}\ m^3 \quad (3)$$

The lattice distortion can be calculated by the following relation (4)

$$U = \frac{a}{c}$$
$$\text{i.e, } U = 1.20 \quad (4)$$

The specific surface area of the crystal can be calculated by the following relation (5)

$$S = \frac{6}{\rho D}\ (m^2/g) \quad (5)$$

The specific surface area of the as prepared SnO_2 powdered particle is 81.24 m^2/g.

3.2. FTIR Spectroscopic studies

The FT-IR spectrum of SnO2 was recorded in 400 – 4000 cm-1 using Shimadzu 8400S FTIR spectrometer and is shown in Fig. 2. The FTIR supports the presence of tin hydroxyl and Tin Oxide functional groups available in SnO_2 nanoparticles. The sharp peak at a low wavenumber of 620 cm^{-1} was due to the anti-symmetric vibration of O-Sn-O [25-28] and also attributed to the oxide-bridge functional group [29]. The peak around 1019cm^{-1} is due to Sn(OH) vibrations [30]. Thus the FTIR spectrum confirms the presence of the Sn-O bond and O-H group. The peak at wave number 1314 cm^{-1} may be due to C–N stretching [31]. The peak at 1399 cm^{-1} refers to the N-H deformation of Ammonia [32]. The band, which appears at 1642 cm^{-1}, indicates that the O-H bond. The absorption band at 2925 cm^{-1} was due to asymmetric C-H and symmetric C-H stretching vibrations [33].

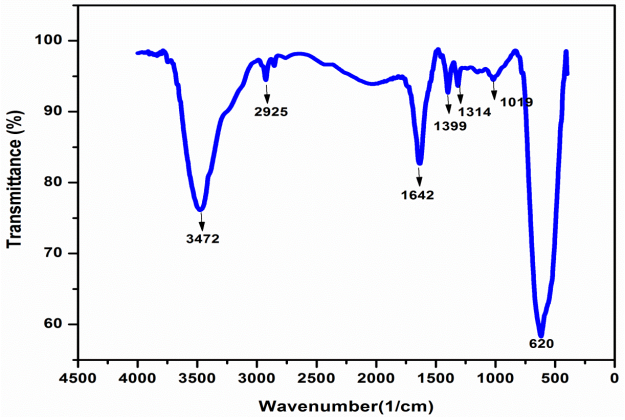

Fig. 2. FT-IR spectra of SnO_2 nanoparticles (color online)

The assignment matches very well with those reported in the literature [33]. The band at 2922cm^{-1} was assigned to C-H stretching vibrations [27]. The top at 1635cm^{-1} relates to extending vibrations of water particles or hydroxide bunches retained at the outside of Tin oxide [27]. The band around 1400 cm^{-1} was allocated to NH disfigurement of smelling salts and the NH extending vibration [32]. The top at wave number 1364 cm^{-1} and is credited to C–N extending [31]. The peak around 1021cm^{-1} is due to Sn (OH) vibrations[34]. The band at 625cm^{-1} refers to Sn – O stretching modes of Sn-O-Sn [32]. The top at wave number 1364 cm^{-1} and is credited to C–N extending [31]. The peak around 1021cm^{-1} is due to Sn (OH) vibrations [34]. The band at 625cm^{-1} refers to Sn – O stretching modes of Sn-O-Sn [32].

3.3. UV - Visible Spectroscopic studies

UV-Vis spectrum is a tool used for examining the optical properties of nano-sized particles. Fig. 3 shows the UV-visible absorption spectrum. The UV- absorption edge gives a reliable estimate of the bandgap of any system. The sample's optical properties can be studied by finding the absorbance, transmittance, and bandgap of the sample. It can be seen from the spectrum that the SnO_2 nanoparticles showed strong absorption from 268 nm to 363 nm in the UV region. i.e., absorption increases from 268 nm to 347 nm, and the maximum absorption was found to be at 347 nm in the UV region. From the UV - Visible Spectroscopic data, a graph was drawn by plotting hν along the x-axis and $(\alpha h\nu)^2$ along the y-axis, called the Tauc plot, and is shown in Fig 4.

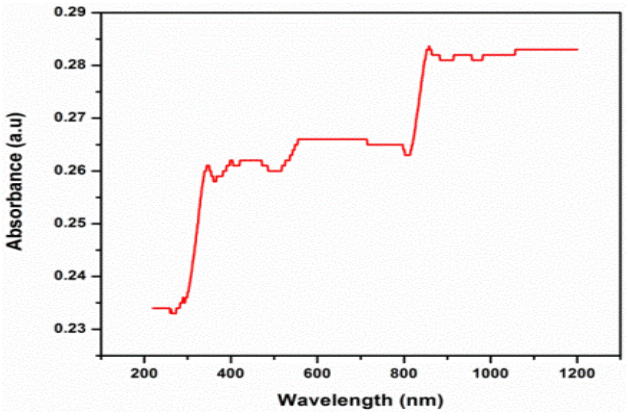

Fig. 3. UV-Visible absorption spectrum of SnO_2 nanoparticles (color online)

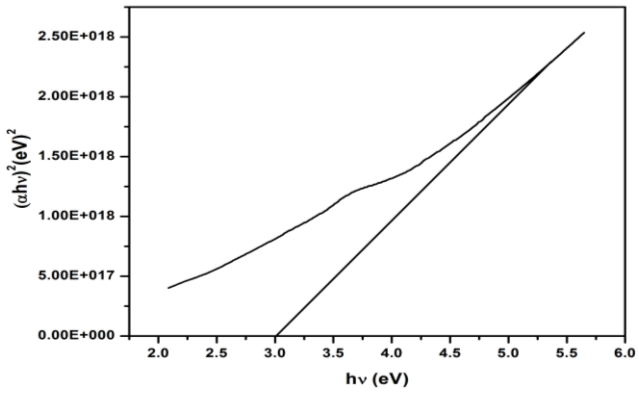

Fig. 4. Tauc plot of SnO_2 nanoparticles

The α was dictated by utilizing the connection α = 2.303 log (abs)/t, where t-is the size of the molecule (nm) and abs - is the absorbance. The connection between the assimilation coefficient (α) and the episode photon vitality hυ can be composed as $\alpha h\upsilon = A(h\upsilon - E_g)^{1/2}$ where A is a constant and E_g is the bandgap energy of the materials. The absorption coefficient can also be calculated using the formula $\alpha = 2.303 \times 10^3 A\rho/Lc$ where A is the absorbance, ρ is the real density of SnO_2 ($\rho = 6.95 g/cm^3$), L is the path length of quartz cell (1cm), and c is the concentration of Tin Oxide. The optical band gap (E_g) was calculated from the extrapolation of the linear part of the Tauc plot. The value of the bandgap of SnO_2 nanoparticles was found to be 3eV. The above value of E_g has been likened to the formation of nanostructures of SnO_2, and the bandgap value shows an agreement with the reported papers. [35].

According to N. Ahmad et al. [36], for SnO_2 nanoparticles, the absorption peak was found at 340 nm corresponding to the bandgap of 3.67 eV.

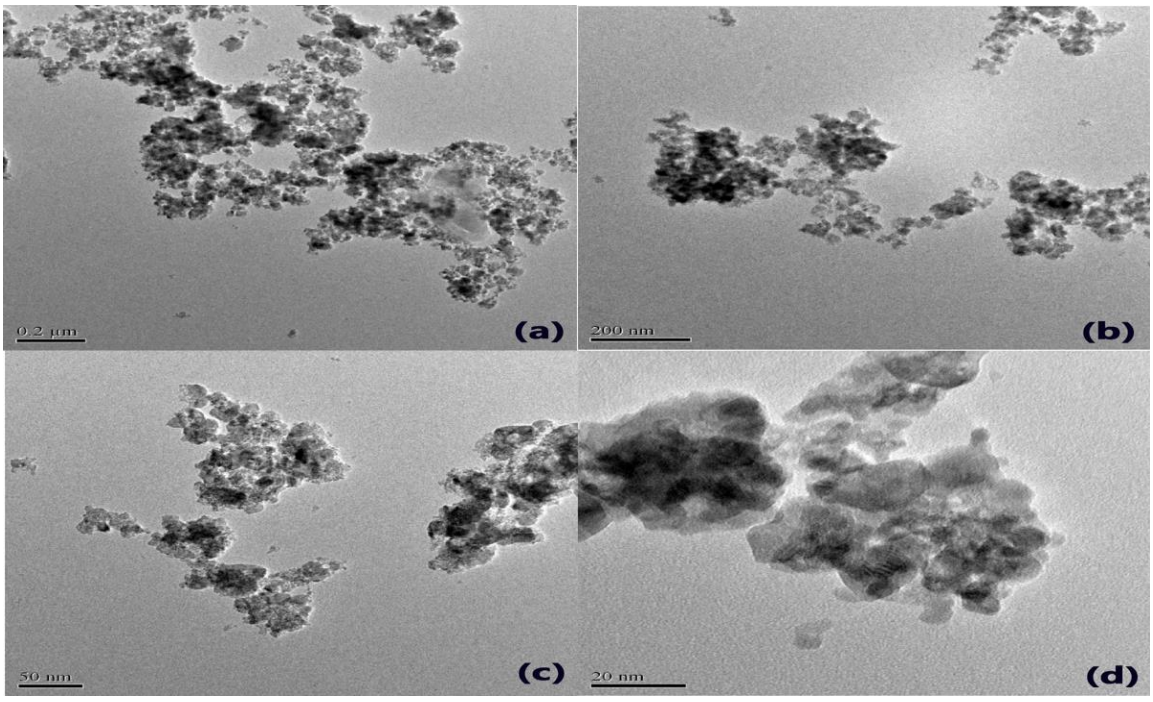

Fig. 5 (a), (b), (c) & (d) HRTEM image of SnO_2 nanoparticles

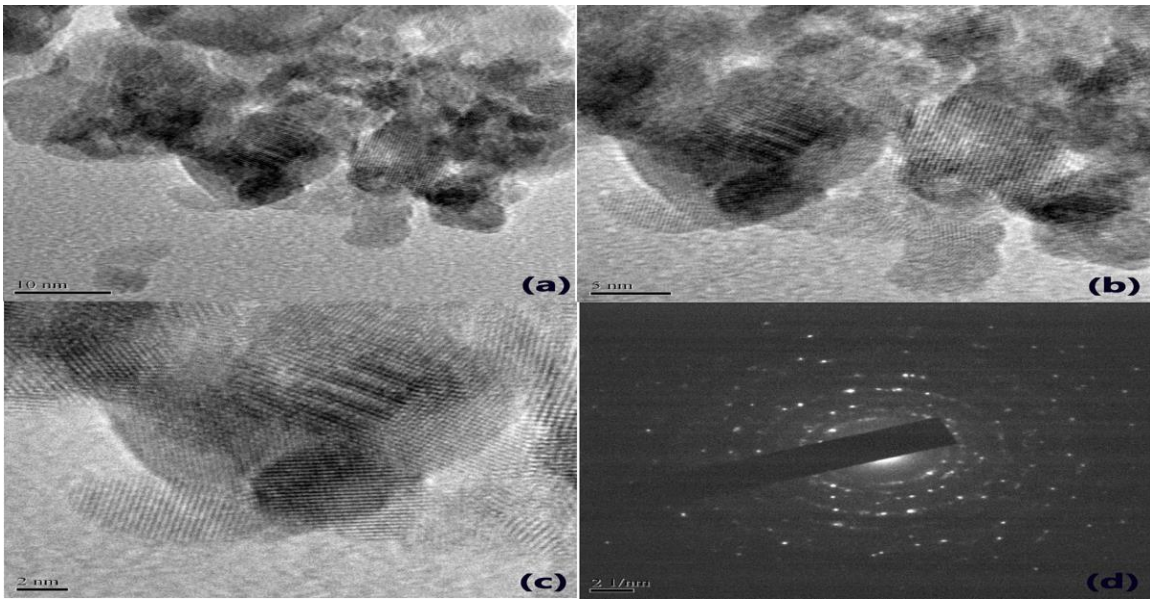

Fig. 6. (a), (b), (c) HRTEM image of SnO_2 nanoparticles, (d) SAED pattern of SnO_2 nanoparticles

3.4. Morphological studies – HRTEM

The particle size and morphology of Tin Oxide nanoparticles from the HRTEM micrographs are shown in Figs. 5(a), (b), (c), (d) and 6 (a), (b), (c). The presence of spherical-shaped particles with particle size range from 10nm to 21 nm was observed. The particle size observed from the HRTEM micrograph matches well with the particle size calculated from the XRD investigation. These results confirmed the formation of crystalline Tin Oxide nanoparticles.The corresponding SAED pattern of SnO_2 nanoparticles is shown in Fig. 6 (d). SAED pattern provides rings made up of bright spots, denoting the crystalline nature of the prepared samples with nano size. The bright image in the SAED pattern confirms the spherical shape of SnO_2 nanoparticles and the narrow distribution of particle size. The HRTEM image of SnO_2 nanoparticles exhibited the irregular circular-like morphology with the molecule size in the range of 7-8 nm, which agrees with the XRD investigation as explained by

S. Gnanam et al. [38]. HRTEM micrograph of SnO_2 nanoparticles prepared by A. S. Lanje et al. [38] observed that the grain size was nearly 25 nm. It was slightly more significant than the crystallite size obtained from XRD analysis (21 nm) using Scherrer's formula, and the SAED image indicates that the particles are highly crystalline. The existence of mono scattered round formed particles with sizes ranging from 76 nm was measured [39].

3.5. Determination of ac conductivity

Fig. 7 has shown ac conductivity with varying angular frequency for SnO_2 nanoparticles at different temperatures. The ac conductivity of SnO_2 nanoparticles was calculated from the experimental data taken from dielectric measurement using the relation,

$$\sigma_{ac} = \varepsilon_0 \varepsilon_r \omega \tan\delta \quad (6)$$

where ε_0 is the permittivity of free space (8.85×10^{-12} Farad/metre), ε_r is the dielectric constant, ω is the angular frequency, and tan δ is the loss factor. It can be observed from the figure that as the frequency increases, ac conductivity also increases [40]. i.e., initially, the ac conductivity remains constant up to 1 KHz. Above 1 KHz, it increases gradually up to 40 kHz and then increases rapidly from 40 – 620 KHz. It is observed from the figure that SnO_2 nanoparticles show frequency dependence behavior of conductivity. According to Jasneet Kaur et al. [44], the value of ac conductivity increases with increasing frequency. The ac conductivity is found to be frequency-dependent in the low-frequency region. The high-frequency area is found to be frequency-independent. The variation of conductivity at high frequencies may be due to the electrode polarization [40].

The conductivities are found to increase with an increase in temperatures. This low-frequency variation is due to the space charge polarization. A frequency-independent conductivity is measured in the mid angular frequency area. The conductivity variations are less predominant at low frequencies and shift to higher frequencies for different temperatures. In other words, the bulk relaxation shifts to higher frequencies with an increase in temperature.

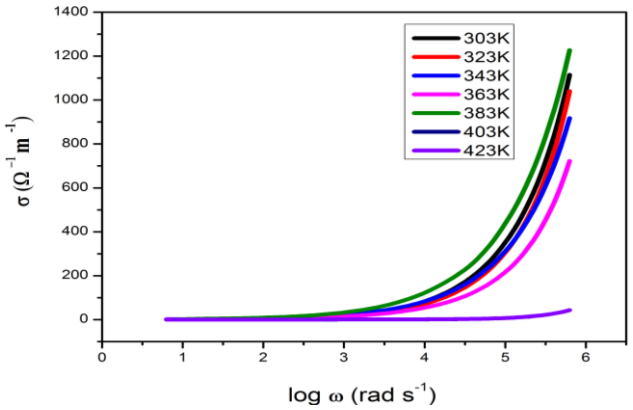

Fig. 7. Log ω Vs ac conductivity of SnO_2 nanoparticles at different temperatures (color online)

3.6. Dielectric studies

The real and imaginary dielectric constants (ε' and ε'') were measured for the SnO_2 nanoparticles to confirm whether they are frequency dependent. Figs. 8 and 9 show the variation of dielectric constant (Real and Imaginary) with varying frequencies of SnO_2 nanoparticles at different temperatures. It is observed from the figure that the value of dielectric constant decreases with increasing frequency. i.e., the dielectric constant decreases rapidly up to 10 KHz. The rapid decrease of dielectric constant at lower frequency up to 10 KHz may be due to space-charge polarization. i.e, electron hopping occurs in this region. However in the mid frequency region from 10 KHz to 1 MHz, the dielectric constant remains constant hence no dispersion.The frequency dependent dielectric behavior can be explained as follows. According to the Maxwell-Wagner model [41], the dielectric medium consists of good conducting grains and poor conducting grain boundaries separate them. On applying the external electric field, the charge carriers undergo migration and accumulate on the grain boundaries. Due to these accumulated charges, polarization occurs in large magnitude and hence higher the dielectric constant. The decrease in dielectric constant is due to the polarizability induced by grain boundaries which lag behind the applied field at higher frequencies [42, 43]. Fig 10 shows the variation of dielectric loss (tanδ) with varying frequencies of SnO_2 nanoparticles at different temperatures from 303K to 363K. The dielectric loss tangent was proportional to the loss of energy (dissipation of heat energy) from the applied field into the sample. As the frequency of the external electric field increases, the value of tan δ for SnO_2 nanoparticles decreases quickly up to 1KHz. The decrease of tanδ with increased frequency can be explained by the Koop's model [44]. According to this model, the rapid decrease of tan δ was due to the lower conductivity value and the grain boundary was dominant.

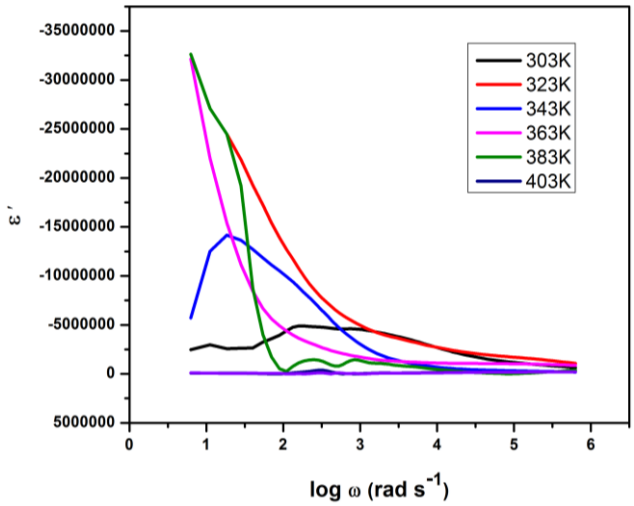

Fig. 8. Variation of dielectric constant (real) with frequency at different temperatures (color online)

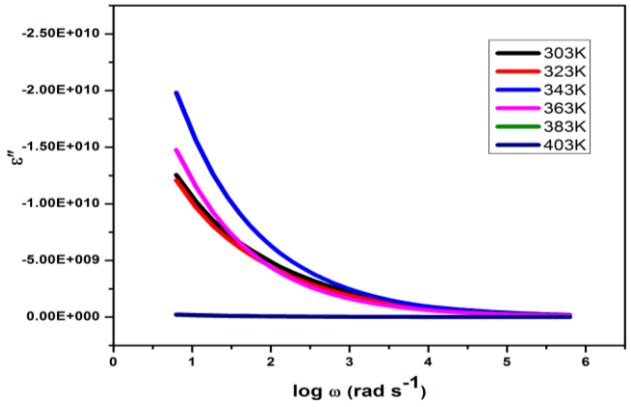

Fig. 9. Variation of dielectric constant (imaginary) with frequency at different temperatures (color online)

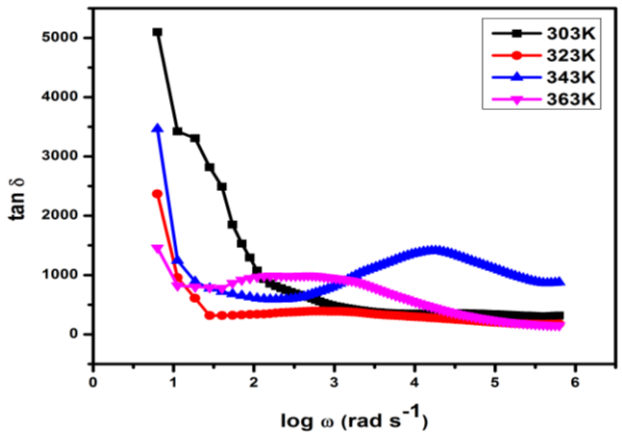

Fig. 10. Log ω Vs tanδ at different temperatures (color online)

4. Conclusion

SnO_2 nanoparticles have been prepared by microwave-assisted solution technique. The structural parameters of the SnO_2 nanoparticles, namely, crystallite diameter, lattice parameters, lattice distortion, cell volume, and specific surface area of the samples, were calculated using the XRD technique. The XRD pattern of SnO_2 nanoparticles shows that the prepared samples are tetragonal crystalline structures. The particle size of SnO_2 nanoparticles were calculated using the value of FWHM(β) from the most intense XRD peaks using the Debye-Scherrer formula and the size of the SnO_2 nanoparticles was found to be in the range of 10-21nm. The FT-IR spectra of SnO_2 nanoparticles were recorded. The functional groups of SnO_2 nanoparticles were identified from FT-IR spectra. The UV-Visible absorption spectra of SnO_2 nanoparticles were recorded, and the bandgap energy was calculated from the Tauc plot. The HRTEM micrographs indicate that the SnO_2 nanoparticles were formed with the particle size of 21nm, which matches XRD results. The impedance spectral studies of the nanocrystalline SnO_2 samples have been carried out. The Cole-Cole plots of the above materials revealed the semiconducting nature of the material. The ac conductivity of the materials showed an exponential increase with the frequency of the applied field at different temperatures. It can be observed from the figure that as the frequency increases, ac conductivity also increases. Hence it was observed that the SnO_2 nanoparticle shows the frequency-dependent behavior of conductivity.

References

[1] M. Batzill. U. Diebold, Prog. Surf. Sci. **79**, 47 (2005).
[2] N. G. Deshpande, Y. G. Gudage, R. Sharma, J. C. Vyas, J. B. Kim, Y. P. Lee, Sensors and Actuators B Chemical, **138**(1), 76 (2009).
[3] H. J. Snaith, C. Ducati, Nano Letters **10**(4), 1259 (2010).
[4] L. Li, C. Liu, Phys. Chem. C **114**, 1444 (2010).
[5] Y. Liu, Y. Liu, Y. Guo, J. Xu, X. Xu, X. Fang, J. Liu, W. Chen, H. Arandiyan, X. Wang, Ind. Eng. Chem. Res. **57(**42), 14052 (2018).
[6] R. D. Sanjay, S.P. Gaikwad, Violet Samuel, V. Ravi, Bull. Mater. Scie. **27**, 221 (2004).
[7] Y. Liu, E. Koep, M. Liu, Chem. Mater. **17**, 3997 (2005).
[8] S. C. Vella Durai, E. Kumar, D. Muthuraj, V. Bena Jothy, J. Nano- Electron. Phys. **12**(3), 03011 (2020)
[9] W. A. Farooq, S. D. Khan, S. M. Ali, M. Aslam, J. Optoelectron. Adv. M., **18(**7-8), 712 (2016).
[10] L. Wang, Z. Wang, J. Zhao, Z. Yuan, H. Yang, M. Zhao, Mater. Chem. Phys. **59**, 171 (1999).
[11] J. W. Park, D. S. Jung, M. E. Seo, S. Y. Kim, W. J. Moon, C. H. Shin, G. Seo, Microporous Mesoporous Mater. **112**, 458 (2008).
[12] Z. Amara, M. Khadraoui, R. Miloua, M. N. Amroun, K. Sahraoui, J. Optoelectron. Adv. M. **22**(3-4), 163 (2020).
[13] J. Gajendiran, V. Rajendran, J. Optoelectron. Adv. M. **15(**9-10), 1059 (2013).
[14] E. Comini, Anal. Chem. Acta **568**, 28 (2006).
[15] T. Krishnakumar, R. Jayaprakash, M. Parthibavarman, A. R. Phani, V. N. Singh, B. R. Mehta, Mater Lett. **63**, 896 (2009).
[16] C. Serin, N. Serin, S. Karadeniz, H. Sari, N. Tugluoglu, O. Pakma, J. Non-Cryst. Solids **352(**3), 209 (2005).
[17] Baohua Zhang, Xiaoyuan Yu, Chunyu Ge, Xianming Dong, Yueping Fang, Zesheng Li, Hongqiang Wang, Chem. Commun. **46**, 9188 (2010).
[18] Weigen Chen, Qu Zhou, Fu Wan, Tuoyu Gao, Journal of Nanomaterials **2012**, 1 (2012).
[19] S. C. Vella Durai, E. Kumar, Journal of Ovonic Research **16(**3), 173 (2020).
[20] G. M. Paulo, L. M. Mario, M. Sergio, Tebcherani, Nanopart Res. **14**, 750 (2012).
[21] K. Suraj, Tripathy, Amrita Mishra, Sandeep Kumar Jha, Rizwan Wahab, A. Abdulaziz, Al- Khedhairy, Mater Sci: Mater Electron **24**, 2082 (2013).
[22] T. Krishnakumar, R. Jayaprakash, V. N. Singh, B. R. Mehta, A. R. Phani, Journal of Nano Research

4, 91 (2008).
[23] R. R. Kasar, N. G. Deshpande, Y. G. Gudage, J. C. Vyas, R. Sharma, Physica B **403**, 3724 (2008).
[24] A. A. Cirera, Vila, A. Cornet, J. R. Morante, Mater. Sci. Eng. C **15**, 203 (2001).
[25] C. M. Liu, X. T. Zu, W. L Zhou, Phys. Condens. Matter **18**, 6001 (2006).
[26] A. Punnoose, J. Hays, A. Thuber, M. H. Engelhard, R. K. Kukkadapu, C. Wang, V. Shutthanandan, S. Thevuthasan. Phys. Rev. B **72**, 54402 (2005).
[27] B. T. Farrukh, Heng, Adnan, Chem. **84**, 537 (2010).
[28] S. Y. Ho, A. S. W. Wong, G. W. Ho, Cryst. Growth. Des. **9**(2), 732 (2009).
[29] Lin Yung-Jen, Wu Ching-Jiunn, Surf Coat. Technol. **88**, 239 (1996).
[30] L. Abello, B. Bouchu, A. Gaskov, S. Koudryavtseva, G. Lucazeau, M. Roumyantseva, Solid State Chem. **135**, 78 (1998).
[31] S. B. Kondawar, S. P. Agrawal, S. H. Nimkar, H. J. Sharma, P. T. Patil, Adv. Mat. Lett. **3**(5), 393 (2012).
[32] S. Blessi, M. Maria Lumina Sonia, S. Vijayalakshmi, S. Pauline, Int. Chem Tech. Research **6**(3), 2153 (2014).
[33] J. Vivekanandan, V. Ponnusamy, A. Mahudeswaran, P. S. Vijayanand, Archives of Applied Science Research **3**(6), 147 (2011).
[34] G. P. Bharat, K. P. Sandip, S. K. Sanjay, International Journal of Innovative Pharmaceutical Sciences and Research **2**(9), 2061 (2014).
[35] S. Gnanam, V. Rajendran, Digest Journal of Nanomaterials and Biostructures **5**(3), 699 (2010).
[36] N. Ahmad, S. Khan, J. Alloys Compd. **720**, 502 (2017).
[37] K. S. Ashok, T. N. Umesh, Advances in Nanoparticles **2**, 66 (2013).
[38] S. Gnanam, V. Rajendran, Journal of Physical Sciences **17**, 185 (2013).
[39] T. Logeswaran, M. Parthibavarman, Nano Vision **3**(2), 54 (2013).
[40] S. C. Vella Durai, E. Kumar, D. Muthuraj, Bull. Chem. Soc. Ethiop. **35**(1), 151(2021).
[41] K. W. Wagner, Am. J. Phys. **40**, 317 (1973).
[42] N. Ahmad, S. Khan, M. M. N. Ansari, Ceram. Int. **44**, 15972 (2018).
[43] N. Ahmad, S. Khan, M. Mohsin, N. Ansari, M. M. N. Ansari, Mater. Res. Express **5**, 035045 (2018).
[44] Jasneet Kaur, Indian Journal of Pure and Applied Physics **50**, 57 (2012).

*Corresponding author: kumarnano@gmail.com